

Factors Governing the Protonation State of Zn-Bound Histidine in Proteins: A DFT/CDM Study

Yen-lin Lin[†] and Carmay Lim^{*†‡}

Contribution from the Institute of Biomedical Science, Academic Sinica, Taipei 11529, Taiwan R.O.C., and Department of Chemistry, National Tsing Hua University, Hsinchu 300, Taiwan R.O.C.

Received October 1, 2003; E-mail: carmay@gate.sinica.edu.tw

Abstract: We have performed systematic theoretical studies to elucidate the factors governing the His protonation/deprotonation state in Zn-binding sites, especially those containing the ubiquitous Zn–His–Asp/Glu triad. Specifically, we have addressed the following three questions: (1) How does the transfer of the Zn-bound His imidazole proton to the second-shell Asp/Glu carboxylate oxygen depend on the composition of the other first-shell ligands and the solvent accessibility of the metal-binding site? (2) Can any second-shell ligand with a proton acceptor group such as the backbone carbonyl oxygen also act as a proton acceptor? (3) What is the effect of the Asp/Glu in the Zn–His–Asp/Glu triad on the Zn-bound water protonation state? To address these questions, we used a combination of quantum mechanical and continuum dielectric methods to compute the free energies for deprotonating a Zn-bound imidazole/water in various Zn complexes. The calculations show that whether the Zn-bound His is protonated or deprotonated depends on (1) the solvent accessibility of the metal-binding site, and (2) the Lewis acid ability of Zn, which is indirectly determined by both the first- and the second-shell Zn ligands. The calculations also show that the effect of the Zn–His–Asp/Glu interaction on the nucleophilicity of the Zn-bound water depends on the solvent accessibility of the catalytic Zn site. Furthermore, they show that the Asp/Glu side chain in the Zn–His–Asp/Glu triad can increase the negative charge of its partner, His, and create an anionic hole that may stabilize a cation in buried cavities, provided that the Zn complex is cationic/neutral. The findings of this work are in accord with available experimental data.

Introduction

Zinc is an essential trace metal that is known to play important catalytic and/or structural role(s) in biological systems.^{1–17} It is an essential cofactor of many metabolic enzymes and transcription factors. Interestingly, from a survey of Zn-containing proteins in the Protein Data Bank,¹⁸ the Asp/Glu

carboxylate side chain has been found to be the most common partner of the Zn-bound His.^{3,4,10,19} In particular, the Zn–His–Asp/Glu triad (Figure 1) has been found in all three types of catalytic zinc cores such as the [Zn(H₂O/OH)(His)₃] site in human carbonic anhydrase II,²⁰ the [Zn(H₂O/OH)(Asp/Glu)(His)₂] core in carboxypeptidase A,²¹ and the [Zn(H₂O/OH)(Cys)₂(His)] site in alcohol dehydrogenase.²² Previous studies have suggested that the Zn²⁺–His[–]–Asp/Glu(H)⁰ triad is energetically more favorable than the Zn²⁺–His⁰–Asp/Glu[–].^{23,24} Here, we show that whether the imidazole proton remains on the Zn-bound His or is transferred to the second-shell Asp/Glu depends on the nature of the other Zn ligands (including the Zn-bound water protonation state), which govern the Lewis acid ability of Zn(II), as well as the solvent accessibility of the metal-binding site. We also discuss the various roles of the Asp/Glu in the Zn–His–Asp/Glu triad and their biological significance.

To rationalize the ubiquitous presence of Asp/Glu in the Zn–His–Asp/Glu triad in various Zn-essential enzymes, several

[†] Institute of Biomedical Science.

[‡] National Tsing Hua University.

- (1) Christianson, D. W. *Adv. Protein Chem.* **1991**, *42*, 281.
- (2) Coleman, J. E. *Annu. Rev. Biochem.* **1992**, *61*, 897.
- (3) Alberts, I. L.; Nadassy, K.; Wodak, S. J. *Protein Sci.* **1998**, *7*, 1700.
- (4) Christianson, D. W.; Alexander, R. S. *J. Am. Chem. Soc.* **1989**, *111*, 6412.
- (5) Cox, E. H.; Hunt, J. A.; Compher, K. M.; Fierke, C. A.; Christianson, D. W. *Biochemistry* **2000**, *39*, 13687.
- (6) Gockel, P.; Vahrenkamp, H. *Chem. Ber.* **1996**, *129*, 1243.
- (7) Gockel, P.; Vahrenkamp, H.; Zuberbuhler, A. D. *Helv. Chim. Acta* **1993**, *76*, 511.
- (8) Ian, L. A.; Katalin, N.; Shoshana, J. W. *Protein Sci.* **1998**, *7*, 1700.
- (9) Ippolito, J. A.; Baird, T. T.; McGee, S. A.; Christianson, D. W.; Fierke, C. A. *Proc. Natl. Acad. Sci. U.S.A.* **1995**, *92*, 5017.
- (10) Karlin, S.; Zhu, Z.-Y.; Karlin, K. D. *Proc. Natl. Acad. Sci. U.S.A.* **1997**, *94*, 14225.
- (11) Karlin, S.; Zhu, Z.-Y. *Proc. Natl. Acad. Sci. U.S.A.* **1997**, *94*, 14231.
- (12) Kiefer, L. L.; Paterno, S. A.; Fierke, C. A. *J. Am. Chem. Soc.* **1995**, *117*, 6831.
- (13) Laity, J. H.; Lee, B. M.; Wright, P. E. *Curr. Opin. Struct. Biol.* **2001**, *11*, 39.
- (14) McCall, K. A.; Huang, C.-C.; Fierke, C. A. *J. Nutr.* **2000**, *130*, 1437S.
- (15) Predki, P. F.; Sarkar, B. *J. Biol. Chem.* **1992**, *267*, 5842.
- (16) Schwabe, J. W. R.; Klug, A. *Nat. Struct. Biol.* **1994**, *1*, 345.
- (17) Vallee, B. L.; Auld, D. S. *Biochemistry* **1990**, *29*, 5647.
- (18) Abola, E. E.; Sussman, J. L.; Prilusky, J.; Manning, N. O. *Protein Data Bank Archives of Three-Dimensional Macromolecular Structures*; Academic Press: San Diego, 1997; Vol. 277.

- (19) Dudev, T.; Lin, Y. L.; Dudev, M.; Lim, C. *J. Am. Chem. Soc.* **2003**, *125*, 3168.
- (20) Hakansson, K.; Carlsson, M.; Svensson, L. A.; Liljas, A. *J. Mol. Biol.* **1992**, *227*, 1192.
- (21) Teplyakov, A.; Wilson, K. S.; Orioli, P.; Mangani, S. *Acta Crystallogr., Sect. D: Biol. Crystallogr.* **1993**, *49*, 534.
- (22) Cho, H.; Ramaswamy, S.; Plapp, B. V. *Biochemistry* **1997**, *36*, 382.
- (23) Nakagawa, S.; Umeyama, H.; Kitaura, K.; Morokuma, K. *Chem. Pharm. Bull. (Tokyo)* **1981**, *29*, 1.
- (24) El Yazal, J.; Roe, R. R.; Pang, Y.-P. *J. Phys. Chem. B* **2000**, *104*, 6662.

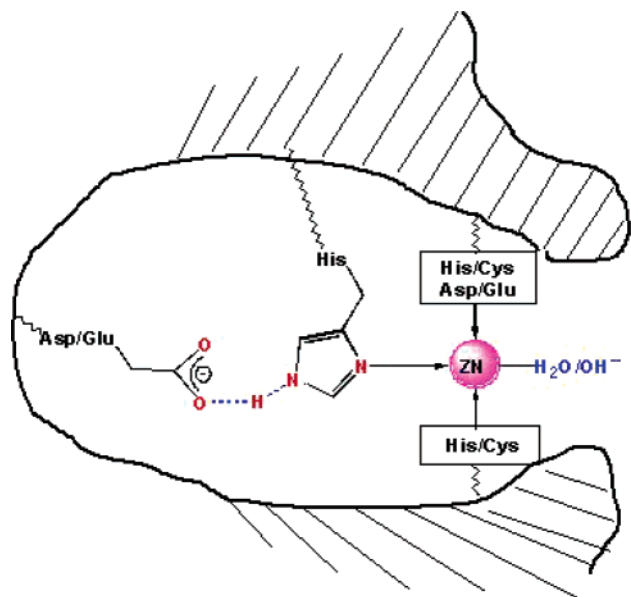


Figure 1. The Zn–His–Asp/Glu triad in Zn-binding proteins.

roles have been proposed for the second-shell Asp/Glu. By interacting with the Zn-bound histidine, the second-shell Asp/Glu has been suggested to (1) enhance the Zn-binding affinity,^{25–27} (2) modulate the basicity/nucleophilicity of metal-bound water (if present),⁴ and (3) act as a proton acceptor, as opposed to a hydrogen-bond acceptor, of the Zn-bound His.^{23,24} The role of the second-shell Asp/Glu in the Zn–His–Asp/Glu triad in promoting Zn binding is supported by various site-directed mutagenesis studies. Mutating Glu¹¹⁷, which is hydrogen bonded to Zn-bound His¹¹⁹ in human carbonic anhydrase II, to alanine decreased the Zn affinity (by ~10-fold) relative to the wild-type protein.^{12,28} In analogy, mutating Asp¹²⁴, which forms hydrogen bonds with Zn- and Cu-bound His ligands in Cu–Zn superoxide dismutase, to asparagine and glycine nearly abolished Zn binding.²⁹ The importance of the His–Asp/Glu interactions in stabilizing the Zn-binding site is also supported by experimental studies on a B1 domain variant of IgG-binding protein G, which contains a designed [Zn(His)₃Cys] binding site: Mutating the second-shell ligands from hydrophobic residues (Val/Leu) to negatively charged residues (Asp/Glu) enhanced metal-binding affinity.³⁰

Experimental evidence for the role of the Asp/Glu in the Zn–His–Asp/Glu triad in modulating the basicity/nucleophilicity of metal-bound water seems ambiguous. The negatively charged Asp/Glu in the Zn–His–Asp/Glu triad has been suggested to destabilize a Zn-bound OH[−],³¹ which should raise the Zn-bound water p*K*_a. Hence, if the negatively charged Asp/Glu side chain were removed, the Zn-bound water p*K*_a should decrease. However, experimental studies on human carbonic anhydrase II show that the Zn-bound water p*K*_a values in the Glu¹¹⁷ → Ala mutant (6.9 ± 0.1)¹² and wild-type protein (6.8 ± 0.1)³²

are identical to within experimental error. This observation has been rationalized by assuming that the Glu¹¹⁷⋯His¹¹⁹ hydrogen bond is compensated by a Cl[−]⋯His¹¹⁹ hydrogen bond based on the X-ray structure of the Glu¹¹⁷ → Ala mutant;³³ thus the electrostatic environment of the Zn, and therefore the Zn-bound water p*K*_a, is maintained in the mutant.

The role of the Asp/Glu in the Zn–His–Asp/Glu triad as a proton acceptor, as opposed to a hydrogen-bond acceptor, was initially suggested by a molecular orbital study on the Zn–His⁶⁹–Asp¹⁴² triad in carboxypeptidase A, where neutral and deprotonated His⁶⁹ were modeled by imidazole (ImH) and imidazolate (Im[−]), respectively, while negatively charged and protonated Asp¹⁴² were modeled by formate (HCOO[−]) and formic acid (HCOOH), respectively.²³ In the absence of zinc and its ligands, the energy minimum of Im[−]⋯HCOOH⁰ is higher than that of ImH⁰⋯HCOO[−] (by 24 kcal/mol), whereas in the presence of zinc and other first-shell ligands, the energy minimum of Zn²⁺–ImH⁰⋯HCOO[−] is higher than that of Zn²⁺–Im[−]⋯HCOOH⁰ (by 3 kcal/mol). The finding that the proton may transfer from a Zn-bound imidazole to a carboxylate oxygen is also supported by gas-phase proton dissociation energies of imidazole in the presence and absence of Zn (computed at the B3LYP/6-311+G(d,p) and MP2/6-311+G(d,p) levels);³⁴ The Zn²⁺–Im[−]⋯MeCOOH⁰ triad is more stable than the Zn²⁺–ImH⁰⋯MeCOO[−] motif in the absence and presence of a Zn-bound hydroxide.²⁴ However, this trend is reversed when the second-shell free carboxylate oxygen is hydrogen bonded to a third-shell water molecule: First principles quantum chemical calculations on various models of the Zn–His⁶⁷–Asp⁴⁹–H₂O quartet of horse liver alcohol dehydrogenase bound to the NAD⁺ cofactor show that, by including a third-shell water molecule, the complex containing Zn²⁺–ImH⁰⋯MeCOO[−]⋯H₂O is energetically more stable than that containing Zn²⁺–Im[−]⋯MeCOOH⁰–H₂O.³⁵

The above findings that the absence of a third-shell water molecule may favor proton transfer from a Zn-bound His to a nearby second-shell carboxylate group, whereas its presence disfavors such a proton transfer, raise several intriguing questions. (1) How does the transfer of the Zn-bound His imidazole proton to the second-shell Asp/Glu carboxylate oxygen depend on the composition/electronic properties of the other first-shell ligands and the solvent accessibility of the metal-binding site? In other words, does the second-shell Asp/Glu side chain act as a hydrogen-bond/proton acceptor for the Zn-bound His in the three general types of catalytic zinc cores, [Zn(H₂O/OH)(His)₃], [Zn(H₂O/OH)(Asp/Glu)(His)₂], and [Zn(H₂O/OH)(Cys)₂–His], and does its role depend on the relative solvent exposure of the metal-binding site? (2) Can any second-shell ligand with a hydrogen-bond acceptor group such as the backbone carbonyl group, which is often found hydrogen bonded to the Zn-bound His,^{3,4,19} also act as a proton acceptor? (3) What is the effect of the Asp/Glu in the Zn–His–Asp/Glu triad on the Zn-bound water protonation state – can it facilitate ionization of the Zn-bound water molecule, and does this role depend on the solvent accessibility of the zinc cavity?

Herein, we address these questions using a combined ab initio and continuum dielectric approach (see Methods). The first- and,

(25) Liljas, A.; Rossmann, M. G. *Annu. Rev. Biochem.* **1974**, *3*, 475.

(26) Kester, W. R.; Matthews, B. W. *J. Biol. Chem.* **1977**, *252*, 7704.

(27) Argos, P.; Garavito, R. M.; Eventoff, W.; Rossmann, M. G.; Branden, C. I. *J. Mol. Biol.* **1978**, *126*, 141.

(28) Kiefer, L. L.; Krebs, J. F.; Paterno, S. A.; Fierke, C. A. *Biochemistry* **1993**, *32*, 9896.

(29) Banci, L.; Bertini, I.; Cabelli, D. E.; Hallewell, R. A.; Tung, J. W.; Viezzoli, M. S. *Eur. J. Biochem.* **1991**, *196*, 123.

(30) Marino, S. F.; Regan, L. *Chem. Biol.* **1999**, *6*, 649.

(31) Christianson, D. W.; Fierke, C. A. *Acc. Chem. Res.* **1996**, *29*, 331.

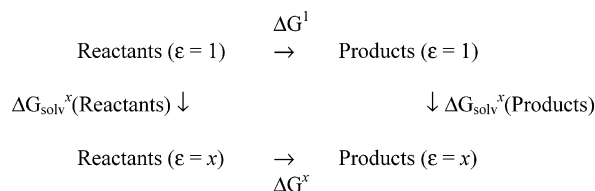
(32) Kiefer, L. L.; Fierke, C. A. *Biochemistry* **1994**, *33*, 15233.

(33) Lesburg, C. A.; Christianson, D. W. *J. Am. Chem. Soc.* **1995**, *117*, 6838.

(34) El Yazal, J.; Pang, Y.-P. *J. Phys. Chem. B* **1999**, *103*, 8773.

(35) Gervasio, F. L.; Schettino, V.; Mangani, S.; Krack, M.; Carloni, P.; Parrinello, M. *J. Phys. Chem. B* **2003**, *107*, 6886.

Scheme 1



in some cases, the second-coordination layers of the metal-binding sites were taken into account explicitly, while the rest of the protein was treated as a continuous medium characterized by a given dielectric constant ranging from 2 to 80. While previous theoretical studies (see above) have focused on the effect of zinc and either the Zn-bound hydroxide²⁴ or a specific set of Zn ligands^{23,35} on the ImH protonation state, we have carried out a systematic study of how the protonation state of the Zn-bound His in representative catalytic zinc cores depends on the Zn site's solvent accessibility, and the other first- (His, Asp/Glu, Cys, and OH⁻) and second-shell ligands (Asp/Glu and backbone peptide). The various roles of the second-shell Asp/Glu as well as the biological significance of the Zn–His–Asp/Glu triad are discussed.

Methods

Models Used. We modeled the common catalytic Zn²⁺-binding sites in proteins,³ viz., [Zn(H₂O/OH)(His)₃], [Zn(H₂O/OH)(Asp/Glu)(His)₂], and [Zn(H₂O/OH)(Cys)₂(His)] cores. The side chains of histidine, aspartic acid/glutamic acid, and cysteine were modeled by imidazole/imidazolate (ImH/Im⁻), acetic acid/acetate (MeCOOH/MeCOO⁻), and methyl thiolate (MeS⁻), respectively, while the backbone peptide group was modeled by MeCONHMe.

Reaction Free Energies, ΔG^x . For a given environment characterized by a dielectric constant $\epsilon = x$, the reaction free energy, ΔG^x , was calculated using the thermodynamic cycle in Scheme 1. ΔG^1 is the gas-phase reaction free energy, while ΔG_{solv}^x is the free energy for transferring a molecule in the gas phase to a continuous medium characterized by a dielectric constant, x . Thus, the reaction free energy in an environment modeled by dielectric constant x , ΔG^x , can be computed from:

$$\Delta G^x = \Delta G^1 + \Delta G_{\text{solv}}^x(\text{products}) - \Delta G_{\text{solv}}^x(\text{reactants}) \quad (1)$$

Gas-Phase Free Energies, ΔG^1 . All of the gas-phase free energy calculations were carried out using the Gaussian 98 program,³⁶ and ΔG^1 was computed according to:

$$\Delta G^1 = \Delta E_{\text{elec}} + \Delta E_{\text{T}} + \Delta PV - T\Delta S \quad (2)$$

where ΔE_{elec} , ΔE_{T} , ΔPV , and ΔS are the differences in the electronic energy, thermal energy, work term, and entropy between the product(s) and reactant(s), respectively. Note that the thermal energy includes the zero-point energy.³⁷ Unless stated otherwise, the geometries of the

molecules were fully optimized using the Slater exchange functional^{38–40} with the Vosko–Wilk–Nusair⁴¹ correlation functional (S-VWN) and the SDD^{42,43} basis set (see next section). For each fully optimized structure, vibrational frequencies were evaluated at the same level of theory – no imaginary frequency was found in any of the fully optimized molecules. The S-VWN/SDD frequencies were scaled by an empirical factor of 0.9833⁴⁴ and used to compute the thermal energy and vibrational entropy. Based on the S-VWN/SDD geometry of a molecule, E_{elec} was estimated by a single-point calculation at the MP2/6-31+G(d) level (see below).

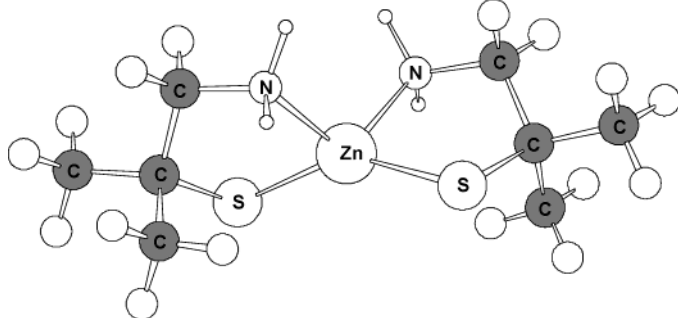
Determining the Optimal Theory/Basis Set Level for Geometry Optimization. To obtain reliable geometries of nitrogen- and sulfur-containing Zn-binding cores, the Cambridge Structure Database⁴⁵ (CSD) was searched for X-ray structures of Zn²⁺ bound to sulfur- and nitrogen-containing ligands that can be used to calibrate the predicted geometries. Bis-(2-amino-1,1-dimethylethanolato)-Zn(II) complex (CSD code AMETZN, Table 1), whose structure has been solved to an *R*-factor of 6.3%,⁴⁶ was selected for geometry calibration. It was fully optimized using Hartree–Fock (HF), B3-LYP,^{47–49} B3-P86,^{47,50} or S-VWN in combination with the 6-31+G(d), 6-311++G(d,p), 6-31+G(d)/SDD (SDD only for Zn), or SDD basis sets (Table 1).

Comparison of the resulting geometries with the X-ray structure in Table 1 shows that among the various methods, S-VWN/SDD yielded the closest agreement with the experimental bond distances with a root-mean-square deviation (rmsd) of 0.025 Å. It also yielded reasonable angles with a rmsd of 1.6°. As compared to S-VWN/SDD, the B3-P86 functional with the same SDD basis set or the same S-VWN functional with the 6-31+G(d) basis yielded better agreement with experiment for the bond angles with a rmsd \leq 0.45°, but slightly worse agreement for the bond distances with a rmsd around 0.035–0.036 Å. However, S-VWN/6-31+G(d) underestimated the experimental Zn–S distance (2.295 \pm 0.004 Å) by 0.063 Å, while B3-P86/SDD overestimated the experimental Zn–N distance (2.062 \pm 0.01 Å) by 0.069 Å. Hence, these two methods may not be optimal for geometry optimization of the common catalytic Zn cores containing Zn bound to S(Cys) and/or N(His). In contrast to the S-VWN/6-31+G(d) and B3-P86/SDD methods, S-VWN/SDD yielded both Zn–S (2.260 Å) and Zn–N (2.070 Å) distances that are close to the respective experimental range with the largest deviation from the experimental distances found for the cyclic C–C bond. The latter is underestimated by 0.041 Å, which in turn may account for the underestimation of the computed Zn–S–C angle. Note, however, that the Zn-binding sites modeled in this work do not contain a cyclic C–C bond.

As found in this work, the S-VWN functional has been found to be adequate for geometry optimization of metal-containing compounds in previous works. It yielded the best bond lengths for a set of 41 inorganic molecules as compared to the BLYP and B3-LYP functionals using the 6-311G* basis set.⁵¹ It also yielded the best bond lengths for a set of 20 molecules containing Cu, Ag, and Au as compared to the BPW, B3-PW, BLYP, and B3-LYP functionals with the LANL2DZ basis set.⁵² Furthermore, in our previous work,⁵³ the S-VWN functional

- (36) Frisch, M. J.; Trucks, G. W.; Schlegel, H. B.; Scuseria, G. E.; Robb, M. A.; Cheeseman, J. R.; Zakrzewski, V. G.; Montgomery, J. A., Jr.; Stratmann, R. E.; Burant, J. C.; Dapprich, S.; Millam, J. M.; Daniels, A. D.; Kudin, M. C.; Strain, K. N.; Farkas, O.; Tomasi, J.; Barone, V.; Cossi, M.; Cammi, R.; Mennucci, B.; Pomelli, C.; Adamo, C.; Clifford, S.; Ochterski, J.; Petersson, G. A.; Ayala, P. Y.; Cui, Q.; Morokuma, K.; Malick, D. K.; Rabuck, A. D.; Raghavachari, K.; Foresman, J. B.; Cioslowski, J.; Ortiz, J. V.; Stefanov, B. B.; Liu, G.; Liashenko, A.; Piskorz, P.; Komaromi, I.; Gomperts, R.; Martin, R. L.; Fox, D. J.; Keith, T.; Al-Laham, M. A.; Peng, C. Y.; Nanayakkara, A.; Gonzalez, C.; Challacombe, M.; Gill, P. M. W.; Johnson, B.; Chen, W.; Wong, M. W.; Andres, J. L.; Gonzalez, C.; Head-Gordon, M.; Replogle, E. S.; Pople, J. A. *Gaussian 98*, revision A.5; Gaussian, Inc.: Pittsburgh, PA, 1998.
- (37) Foresman, J. B.; Frisch, E. *Exploring Chemistry with Electronic Structure Methods*, 2nd ed.; Gaussian, Inc.: Pittsburgh, PA, 1996.

- (38) Hohenberg, P.; Kohn, W. *Phys. Rev.* **1964**, *136*, B864.
- (39) Kohn, W.; Sham, L. J. *Phys. Rev.* **1965**, *140*, A1133.
- (40) Slater, J. C. *Quantum Theory of Molecules and Solids. Vol. 4: The Self-Consistent Field for Molecules and Solids*; McGraw-Hill: New York, 1974.
- (41) Vosko, S. H.; Wilk, L.; Nusair, M. *Can. J. Phys.* **1980**, *58*, 1200.
- (42) Fuentealba, P.; Preuss, H.; Stoll, H.; Szentpaly, L. V. *Chem. Phys. Lett.* **1989**, *89*, 418.
- (43) Szentpaly, L. V.; Fuentealba, P.; Preuss, H.; Stoll, H. *Chem. Phys. Lett.* **1982**, *93*, 555.
- (44) Wong, M. W. *Chem. Phys. Lett.* **1996**, *256*, 391.
- (45) Allen, F. H. *Acta Crystallogr., Sect. B* **2002**, *58*, 380.
- (46) Cohen, B.; Mastropaolo, D.; Potenza, J. A.; Schugar, H. J. *Acta Crystallogr., Sect. B* **1978**, *34*, 2859.
- (47) Becke, A. D. *Phys. Rev.* **1988**, *A38*, 3098.
- (48) Lee, C.; Yang, W.; Parr, R. G. *Phys. Rev.* **1988**, *B37*, 785.
- (49) Miehlich, B.; Savin, A.; Stoll, H.; Preuss, H. *Chem. Phys. Lett.* **1989**, *157*, 200.
- (50) Perdew, J. P. *Phys. Rev. B* **1986**, *33*, 8822.
- (51) Bytheway, I.; Wong, M. W. *Chem. Phys. Lett.* **1998**, *282*, 219.
- (52) Legge, F. S.; Nyberg, G. L.; Peel, J. B. *J. Phys. Chem. A* **2001**, *105*, 7905.

Table 1. Calculated and Experimental Structural Parameters for Bis-(2-amino-1,1-dimethylethanethiolato) Zinc Complex^a


| | Zn-S | Zn-N | S-C | N-C | C-C | rmsd ^b | S-Zn-N | Zn-S-C | Zn-N-C | rmsd ^c |
|-------------------------------|-------|-------|-------|-------|-------|-------------------|--------|--------|--------|-------------------|
| HF/6-31+G(d) | 2.305 | 2.208 | 1.849 | 1.473 | 1.536 | 0.067 | 88.0 | 96.7 | 108.7 | 2.78 |
| HF/6-311++G(d,p) | 2.312 | 2.220 | 1.851 | 1.473 | 1.534 | 0.072 | 87.8 | 96.6 | 108.5 | 2.85 |
| HF/6-31+G(d) (SDD for Zn) | 2.296 | 2.211 | 1.849 | 1.473 | 1.536 | 0.068 | 88.1 | 96.9 | 108.6 | 2.82 |
| HF/SDD | 2.316 | 2.177 | 1.908 | 1.489 | 1.542 | 0.055 | 89.6 | 95.6 | 108.7 | 1.73 |
| S-VWN/6-31+G(d) | 2.232 | 2.089 | 1.841 | 1.461 | 1.520 | 0.036 | 91.2 | 93.7 | 108.6 | 0.30 |
| S-VWN/6-311++G(d,p) | 2.233 | 2.103 | 1.839 | 1.461 | 1.517 | 0.039 | 90.8 | 94.0 | 108.4 | 0.63 |
| S-VWN/6-31+G(d) (SDD for Zn) | 2.225 | 2.107 | 1.836 | 1.460 | 1.524 | 0.043 | 90.9 | 94.1 | 108.5 | 0.61 |
| S-VWN/SDD | 2.260 | 2.070 | 1.890 | 1.479 | 1.479 | 0.025 | 92.7 | 90.8 | 108.5 | 1.62 |
| B3-LYP/6-31+G(d) | 2.285 | 2.202 | 1.869 | 1.485 | 1.541 | 0.064 | 89.0 | 96.5 | 108.5 | 2.33 |
| B3-LYP/6-311++G(d,p) | 2.285 | 2.211 | 1.873 | 1.485 | 1.540 | 0.067 | 88.8 | 96.5 | 108.5 | 2.41 |
| B3-LYP/6-31+G(d) (SDD for Zn) | 2.277 | 2.213 | 1.869 | 1.485 | 1.543 | 0.069 | 88.9 | 96.7 | 108.4 | 2.46 |
| B3-LYP/SDD | 2.309 | 2.166 | 1.925 | 1.502 | 1.549 | 0.053 | 90.6 | 94.6 | 108.6 | 0.89 |
| B3-P86/6-31+G(d) | 2.262 | 2.160 | 1.855 | 1.475 | 1.532 | 0.048 | 89.7 | 95.6 | 108.6 | 1.68 |
| B3-P86/6-311++G(d,p) | 2.265 | 2.175 | 1.853 | 1.472 | 1.531 | 0.054 | 89.3 | 95.7 | 108.4 | 1.88 |
| B3-P86/6-31+G(d) (SDD for Zn) | 2.257 | 2.176 | 1.851 | 1.474 | 1.536 | 0.056 | 89.5 | 95.9 | 108.4 | 1.92 |
| B3-P86/SDD | 2.291 | 2.131 | 1.909 | 1.491 | 1.536 | 0.035 | 91.1 | 94.0 | 108.6 | 0.45 |
| EXP(AMETZN) ^d | 2.295 | 2.062 | 1.878 | 1.484 | 1.520 | | 91.4 | 93.3 | 108.8 | |

^a Average values. Bond lengths are in angstroms, and bond angles are in degrees. ^b Root-mean-square deviation of the computed Zn-S, Zn-N, S-C, N-C, and C-C distances from the respective experimental values. ^c Root-mean-square deviation of the computed S-Zn-N, Zn-S-C, and Zn-N-C angles from the respective experimental values. ^d From Cohen et al., 1978.⁴⁶

with the 6-31+G(d), 6-311++G(d,p), or 6-311++G(2d,2p) basis set was found to yield structural parameters for the bis-(ethane-1,2-dithiolato-*S,S'*)-zinc(II) complex⁵⁴ that are significantly closer to the experimental observables than the B-VWN, B3-LYP, and B3-P86 functionals with the same basis set. In particular, S-VWN with the 6-31+G(d) basis set reproduces the experimentally observed ⟨Zn-S⟩ (2.34 ± 0.02 Å), ⟨S-C⟩ (1.81 ± 0.01 Å), and ⟨C-C⟩ (1.50 Å) distances as well as the ⟨S-Zn-S⟩ angles, whereas B-VWN, B3-LYP, and B3-P86 with the same 6-31+G(d) basis set significantly overestimate the ⟨Zn-S⟩ distance by ≥0.6 Å. Increasing the size of the basis set from 6-31+G(d) to 6-311++G(2d,2p) in the B3-LYP calculations yields a ⟨Zn-S⟩ distance of 2.432 Å, which does not improve the agreement with experiment. As the S-VWN/SDD method appears to be optimal for modeling Zn²⁺ bound to nitrogen- and sulfur-containing ligands, it was used to optimize the geometries of all of the molecules studied.

Determining the Optimal Theory/Basis Set Level for Gas-Phase Free Energy Calculations. As the theory/basis set level that produced accurate geometries may not yield the proper gas-phase energies of Zn complexes,⁵³ we determined the optimal theory/basis set for electronic energy calculations by computing the gas-phase free energy for deprotonating imidazolium (ImH₂⁺) to imidazole (ImH) (see Table 2). Although the more relevant reaction to model is deprotonating ImH to imidazolate anion (Im⁻), corresponding to the deprotonation of a Zn-bound imidazole, the experimental gas-phase free energy for ImH → Im⁻ + H⁺ is not available. Based on the fully optimized S-VWN/SDD geometries of ImH₂⁺ and ImH, the respective Δ*E*_{elec} was estimated by a single-point calculation using HF, B3-P86, B3-LYP, MP2, or S-VWN^{55–58} in combination with the 6-31+G(d), 6-311++G(d,p),

Table 2. Gas-Phase Free Energies^a (in kcal/mol) at 298.15 K for ImH₂⁺ → ImH + H⁺

| | 6-31+G(d) | 6-311++G(d,p) | 6-311++G(2d,2p) | SDD |
|--------|-----------|---------------|-----------------|-------|
| HF | 221.4 | 223.6 | 223.6 | 228.5 |
| B3-P86 | 217.9 | 219.5 | 219.7 | 226.2 |
| B3-LYP | 216.8 | 218.6 | 218.8 | 225.4 |
| MP2 | 213.6 | 216.7 | 216.1 | 223.5 |
| S-VWN | 212.0 | 213.2 | 213.3 | 221.0 |

^a Evaluated using S-VWN/SDD geometries and vibrational frequencies with single-point calculations of the energies at different theory levels.

6-311++G(2d,2p), or SDD basis set, and the respective Δ*G*¹ values were computed using eq 2.

Comparison of the resulting gas-phase ImH₂⁺ deprotonation free energies in Table 2 with the experimental number, 214.3 kcal/mol,⁵⁹ shows that among the various methods, MP2/6-31+G(d) yielded the closest agreement with the measured value (to within 0.7 kcal/mol). Although the S-VWN/SDD method can yield reasonably accurate geometries of Zn complexes, it is not the optimal method for yielding deprotonation energies, as the predicted deprotonation ImH₂⁺ free energy overestimated the experimental number by 6.7 kcal/mol. Thus, all gas-phase energy calculations were performed at the MP2/6-31+G(d)/S-VWN/SDD level.

Solvation Free Energies. Δ*G*_{sol}^v was estimated by solving Poisson's equation using finite difference methods.^{60,61} These calculations em-

(53) Dudev, T.; Lim, C. *J. Phys. Chem. B* **2001**, *105*, 10709.

(54) Rao, C. P.; Dorfman, J. R.; Holm, R. H. *Inorg. Chem.* **1986**, *25*, 428.

(55) Saebø, S.; Almlof, J. *Chem. Phys. Lett.* **1989**, *154*, 83.

(56) Frisch, M. J.; Head-Gordon, M.; Pople, J. A. *Chem. Phys. Lett.* **1990**, *166*, 275.

(57) Head-Gordon, M.; Pople, J. A.; J., F. M. *Chem. Phys. Lett.* **1988**, *153*, 503.

(58) Head-Gordon, M.; Head-Gordon, T. *Chem. Phys. Lett.* **1994**, *220*, 122.

(59) Lias, S. G.; Liebman, J. F.; Levin, D. J. *Phys. Chem. Ref. Data* **1984**, *13*.

(60) Gilson, M. K.; Honig, B. *Biopolymers* **1986**, *25*, 2097.

Table 3. Effective Solute Radii for Continuum Dielectric Calculations

| species | $\Delta G_{\text{solv,expt}}^{80}$ kcal/mol | $\Delta G_{\text{solv,calc}}^{80}$ kcal/mol | atom type | R_{eff} Å |
|--|--|--|-------------------|-----------------------|
| ImH | -10.2 ^a | -10.2 | C ^{sp2} | 2.20 |
| | | | N ^{sp2} | 2.00 |
| | | | N ^H | 1.90 |
| | | | H ^C | 1.47 |
| | | | H ^N | 0.23 |
| MeCONHMe | -10.0 ^b | -10.0 | C ^{sp3} | 2.30 |
| | | | O=C | 1.90 |
| MeCOOH | -6.7 ^a | -6.6 | O ^H | 2.03 |
| | | | H ^O | 0.23 |
| MeSH | -1.2 ^c | -1.2 | S ^H | 2.40 |
| | | | H ^S | 0.23 |
| MeCOO ⁻ | -77.7 ^d | -77.6 | O ^{COO-} | 1.60 |
| MeS ⁻ | -75.9 ^e | -75.8 | S ⁻ | 1.91 |
| Im ⁻ | -60.9 ^f | -60.9 | N ⁻ | 2.26 |
| [ZnW ₆] ²⁺ | -229.2 ^g | -229.2 | Zn ²⁺ | 1.40 |
| | | | O ^{H2O} | 1.63 |
| | | | H ^{H2O} | 1.00 |
| [ZnW ₃ OH·W ₂] ⁺ | -104.6 ^h | -104.5 | O ^{OH-} | 1.47 |
| | | | H ^{OH-} | 0.23 |

^a From Wolfenden et al., 1981.⁶³ ^b From Wolfenden, 1978.⁶⁴ ^c From Hine and Mookerjee, 1975.⁶⁵ ^d Using eq 3 with $\text{p}K_{\text{a,expt}}(\text{CH}_3\text{COOH}) = 4.866$ and $\Delta G_{\text{expt}}^1(\text{CH}_3\text{COOH} \rightarrow \text{CH}_3\text{COO}^- + \text{H}^+) = 341.5$ kcal/mol.⁶⁷ ^e Using eq 3 with $\text{p}K_{\text{a,expt}}(\text{CH}_3\text{SH}) = 10.368$ and $\Delta G_{\text{expt}}^1(\text{CH}_3\text{SH} \rightarrow \text{CH}_3\text{S}^- + \text{H}^+) = 352.7$ kcal/mol.⁶⁷ ^f Using eq 3 with $\text{p}K_{\text{a,expt}}(\text{ImH}) = 14.569$ and $\Delta G_{\text{calc}}^1(\text{ImH} \rightarrow \text{Im}^- + \text{H}^+) = 334.4$ kcal/mol.⁸ ^g Using eq 4 with $\Delta G_{\text{solv,expt}}^{80}(\text{Zn}^{2+}) = -484.6$ kcal/mol,⁷⁰ and $\Delta G_{\text{calc}}^1(\text{Zn}^{2+} + 6\text{W} \rightarrow [\text{ZnW}_6]^{2+}) = -255.4$ kcal/mol.⁸ ^h Using eq 3 with $\text{p}K_{\text{a,expt}}(\text{ZnW}_6) = 9.071$ and $\Delta G_{\text{calc}}^1([\text{ZnW}_6]^{2+} \rightarrow \{[\text{ZnW}_3\text{OH}]\cdot\text{W}_2\}^+ + \text{H}^+) = 151.7$ kcal/mol.

ployed a $71 \times 71 \times 71$ lattice centered on the metal cation with a final grid spacing of 0.25 Å, ab initio geometries, and natural bond orbital (NBO) atomic charges.⁶² The low-dielectric region of the solute was defined as the region inaccessible to contact by a 1.4 Å-radius sphere rolling over the molecular surface, which was defined by the effective solute radii, R_{eff} , listed in Table 3 (see below). This region was assigned an internal dielectric constant ϵ_{in} of 2 to account for the electronic polarizability of the solute. Zn-binding sites were characterized by an external dielectric constant ϵ_{out} ranging from 2 to 80. Thus, Poisson's equation was solved with ϵ_{out} equal to 1, 2, 4, or 80 and $\epsilon_{\text{in}} = 2$. The difference between the computed electrostatic potentials in a given dielectric medium ($\epsilon_{\text{out}} = x$) and in the gas phase ($\epsilon_{\text{out}} = 1$) yielded the solvation free energy $\Delta G_{\text{solv},x}$ of the metal complex.

Determining the Effective Dielectric Boundary for Solvation Free Energy Calculations. The effective radii, R_{eff} , for the various atoms listed in Table 3 were obtained by adjusting the CHARMM (version 22)⁷² van der Waals radii to reproduce the experimental hydration free energies as well as the absolute and relative $\text{p}K_{\text{a}}$ values of the model compounds and the metal complexes. First, the CHARMM van der Waals radii of sp^3 carbon (C^{sp3}), sp^2 carbon (C^{sp2}), sp^2 nitrogen (N^{sp2}), protonated nitrogen (N^H), hydroxyl oxygen (O^H), carbonyl oxygen (O=C), S^H, H^C, H^N, H^O, and H^S were simultaneously adjusted to

reproduce the experimental hydration free energies of ImH, MeCONHMe, CH₃COOH, and CH₃SH (see Table 3).

Next, the radii of the imidazolate nitrogen (N⁻), carboxylate oxygen (O^{COO-}), and thiolate sulfur (S⁻) were simultaneously adjusted to reproduce the measured absolute as well as relative $\text{p}K_{\text{a}}$ values of ImH, CH₃COOH, and CH₃SH, which indirectly determine the respective "experimental" hydration free energy of the deprotonated molecule as follows:

$$\Delta G_{\text{solv,expt}}^{80}(\text{A}^-) = \Delta G_{\text{solv,expt}}^{80}(\text{AH}) - \Delta G_{\text{solv,expt}}^{80}(\text{H}^+) + 2.303RT \text{p}K_{\text{a,expt}}(\text{AH}) - \Delta G_{\text{expt}}^1(\text{AH}) \quad (3)$$

In eq 3, $\text{A}^- = \text{MeCOO}^-$, MeS^- , or Im^- ; $\Delta G_{\text{solv,expt}}^{80}(\text{AH})$ is the experimental hydration free energy of the protonated molecule, AH; $\Delta G_{\text{solv,expt}}^{80}(\text{H}^+)$ is the experimental proton hydration free energy (-264.0 kcal/mol⁷³), $\text{p}K_{\text{a,expt}}(\text{AH})$ is the measured solution $\text{p}K_{\text{a}}$ of AH, and $\Delta G_{\text{expt}}^1(\text{AH})$ is the experimental gas-phase free energy for deprotonating AH to A^- and H^+ (see Table 3). In the case of $\text{ImH} \rightarrow \text{Im}^- + \text{H}^+$, the experimental gas-phase free energy is not available; thus $\Delta G^1(\text{AH})$ was estimated using eq 2 with ΔE_{elec} evaluated at the MP2/6-31+G(d)//S-VWN/SDD level (see footnotes of Table 3).

The Zn and water (W) oxygen and hydrogen radii were simultaneously adjusted to reproduce the "experimental" hydration free energy of $[\text{ZnW}_6]^{2+}$, which was estimated from the measured hydration free energy of Zn^{2+} (-484.6 kcal/mol)⁷⁰ and the computed gas-phase free energy for $\text{Zn}^{2+} + 6\text{W} \rightarrow [\text{ZnW}_6]^{2+}$; that is,

$$\Delta G_{\text{solv,expt}}^{80}([\text{ZnW}_6]^{2+}) \approx \Delta G_{\text{solv,expt}}^{80}(\text{Zn}^{2+}) - \Delta G_{\text{calc}}^1(\text{Zn}^{2+} + 6\text{W} \rightarrow [\text{ZnW}_6]^{2+}) \quad (4)$$

As basis set superposition error is likely to be significant in complex formation reactions, a counterpoise correction (30.5 kcal/mol) was applied to the gas-phase binding energy ΔE_{elec} (-353.5 kcal/mol, evaluated at the MP2/6-31+G(d)//S-VWN/SDD level) for $\text{Zn}^{2+} + 6\text{W} \rightarrow [\text{ZnW}_6]^{2+}$. The resulting gas-phase free energy ΔG_{calc}^1 was estimated to be equal to -255.4 kcal/mol.

Our previous work showed that Zn^{2+} changes its coordination number upon deprotonating a Zn-bound water molecule as the hexacoordinated $[\text{ZnW}_3\text{OH}]^+$ complex spontaneously decomposed into a tetrahedral $[(\text{ZnW}_3\text{OH})\cdot\text{W}_2]^+$ complex with two water molecules in the outer sphere.⁷⁴ Thus, the radii for the Zn-bound hydroxide atoms were simultaneously adjusted to reproduce the "experimental" hydration free energy of $[\text{ZnW}_3\text{OH}\cdot\text{W}_2]^+$, which was estimated from eq 3 with $\text{AH} = [\text{ZnW}_6]^{2+}$, using the "experimental" hydration free energy of $[\text{ZnW}_6]^{2+}$ (-229.2 kcal/mol), $\Delta G_{\text{solv,expt}}^{80}(\text{H}^+)$ (-264.0 kcal/mol⁷³), the measured $\text{p}K_{\text{a}}$ of $[\text{ZnW}_6]^{2+}$ (9.071), and the computed gas-phase free energy for deprotonating $[\text{ZnW}_6]^{2+}$ (151.7 kcal/mol).

Results

In interpreting the results below, we emphasize the trend of the free energy change between two sets of reactions, as opposed to the absolute free energy of a single reaction. In this way, systematic errors in the computed free energies for the two reactions will hopefully cancel. In particular, the proton hydration free energy cancels in comparing two deprotonation reactions. Furthermore, errors in the gas-phase energies, ΔE_{elec} , have been minimized by calibrating the theory/basis set employed (see Tables 1 and 2), while errors in the hydration free energies, $\Delta G_{\text{solv}}^{80}$, have been minimized by using effective atomic radii that have been adjusted to reproduce the experi-

- (61) Lim, C.; Bashford, D.; Karplus, M. *J. Phys. Chem.* **1991**, *95*, 5610.
 (62) Reed, A. E.; Curtiss, L. A.; Weinhold, F. *Chem. Rev.* **1988**, *88*, 899.
 (63) Wolfenden, R.; Anderson, L.; Gullis, P. M.; Southgate, C. C. B. *Biochemistry* **1981**, *20*, 849.
 (64) Wolfenden, R. *Biochemistry* **1978**, *17*, 201.
 (65) Hine, J.; Mookerjee, P. K. *J. Org. Chem.* **1975**, *40*, 287.
 (66) Pearson, R. G. *J. Am. Chem. Soc.* **1986**, *108*, 6109.
 (67) Bartmess, J. E.; McIver, R. T., Jr. *Gas-Phase Ion Chemistry*; Academic Press: New York, 1979; Vol. 2.
 (68) *Handbook of Physical Properties of Organic Chemicals*; Howard, P. H., Meylan, W. M., Eds.; Lewis Publishers: Boca Raton, FL, 1997.
 (69) Jencks, W. P.; Regenstein, J. *Handbook of Biochemistry and Molecular Biology*, 3rd ed.; CRC Press: Cleveland, OH, 1976; Vol. I.
 (70) Burgess, M. A. *Metal Ions in Solution*; Ellis Horwood: Chichester, England, 1978.
 (71) Richens, D. T. *The Chemistry of Aqua Ions*; John Wiley & Sons: New York, 1997.
 (72) Brooks, B. R.; Bruccoleri, R. E.; Olafson, B. D.; States, D. J.; Swaminathan, S.; Karplus, M. *J. Comput. Chem.* **1983**, *4*, 187.

- (73) Tissandier, M. D.; Cowen, K. A.; Feng, W. Y.; Gundlach, E.; Cohen, M. H.; Earhart, A. D.; Coe, J. V.; Tuttle, T. R., Jr. *J. Phys. Chem. A* **1998**, *102*, 7787.
 (74) Chao, Y. F.; Deubel, D. V.; Lim, C., in preparation.

Table 4. Effect of the Zn Geometry, First-Shell Ligands, and the Dielectric Medium on the Deprotonation ΔG^x (in kcal/mol) of Zn^{2+} -Bound ImH^a

| reactant | product + H^+ | $\Delta\Delta H^{1,b}$ | $\Delta\Delta G^{1,b}$ | $\Delta\Delta G^{2,b}$ | $\Delta\Delta G^{4,b}$ | $\Delta\Delta G^{80,b}$ |
|--|---|------------------------|------------------------|------------------------|------------------------|-------------------------|
| 1. $[\text{ZnW}_3\text{ImH}]^{2+}$ | $[\text{ZnW}_3\text{Im}]^+$ | 0.0 | 0.0 | 0.0 | 0.0 | 0.0 |
| 2. $[\text{ZnW}_4\text{ImH}]^{2+,c}$ | $[\text{ZnW}_4\text{Im}]^{+,c}$ | 2.1 | 1.8 | 2.2 | 1.8 | 1.1 |
| 3. $[\text{ZnW}_5\text{ImH}]^{2+,c}$ | $[\text{ZnW}_5\text{Im}]^{+,c}$ | 5.4 | 5.3 | 6.7 | 7.1 | 6.8 |
| 4. $[\text{ZnW}_2\text{ImHImH}]^{2+}$ | $[\text{ZnW}_2\text{ImHIm}]^+$ | 8.1 | 8.7 | 7.0 | 6.5 | 7.1 |
| 5. $[\text{ZnW}(\text{ImH})_2\text{ImH}]^{2+}$ | $[\text{ZnW}(\text{ImH})_2\text{Im}]^+$ | 16.3 | 17.4 | 10.4 | 7.2 | 4.5 |
| 6. $[\text{ZnW}_2\text{AceImH}]^+$ | $[\text{ZnW}_2\text{AceIm}]^0$ | 62.4 | 61.5 | 22.5 | 3.2 | -14.8 |
| 7. $[\text{ZnW}_2\text{MeSImH}]^+$ | $[\text{ZnW}_2\text{MeSIm}]^0$ | 65.0 | 63.6 | 25.5 | 6.4 | -12.1 |

^a $x = 1$ corresponds to the gas phase, whereas $x = 80$ represents fully solvent-exposed sites (see Methods). The ΔG^1 values are based on fully optimized S-VWN/SDD geometries of the protonated and deprotonated molecules unless stated otherwise in the text. ^b The computed thermodynamic parameters are relative to those of reaction 1, whose ΔH^1 , ΔG^1 , ΔG^2 , ΔG^4 , and ΔG^{80} values are equal to 179.2, 171.7, 109.3, 72.0, and 20.0 kcal/mol, respectively. ΔG^2 and ΔG^4 are based on the calculated $\Delta G_{\text{solv}}^2(\text{H}^+)$ of -134.4 kcal/mol and $\Delta G_{\text{solv}}^4(\text{H}^+)$ of -200.1 kcal/mol, respectively, while ΔG^{80} is based on the experimental $\Delta G_{\text{solv}}^{80}(\text{H}^+)$ of -264 kcal/mol. ^c C_2 symmetry was imposed during geometry optimization.

mental hydration free energies and $\text{p}K_a$ values of the model compounds and the metal complexes in Table 3. Note that these effective radii implicitly take into account the ambiguity in the atomic charges and thus geometry in solution as well as the neglect of nonelectrostatic forces in computing $\Delta G_{\text{solv}}^{80}$.

Protonation State of Zn-Bound ImH. We first assessed how the protonation state of a Zn-bound histidine depends on the Zn geometry, dielectric medium, and the other first- (His, Cys, Asp/Glu, and OH^-) and second-shell ligands (Asp/Glu and carbonyl backbone peptide).

(1) Effect of the Zn Geometry. Because the Zn coordination number in protein cavities can vary from four to six, we evaluated the effect of the Zn geometry on deprotonating ImH in tetra-, penta-, and hexa-coordinated Zn complexes (Table 4, reactions 1–3). The ΔG^1 value for deprotonating ImH in the penta/hexa-coordinated complexes is more positive (by 2 or 5 kcal/mol) than that in the corresponding tetrahedral complex. The ΔG difference between the penta/hexa-coordinated and tetrahedral Zn complexes remains positive with increasing dielectric constant. These results suggest that penta/hexa-coordinated Zn complexes generally disfavor deprotonation of ImH more so than tetrahedral Zn complexes; hence only tetrahedral Zn complexes were considered below.

(2) Effect of the First-Shell Ligands and the Dielectric Medium. To evaluate the effect of the first-shell ligands on the ImH protonation state in various Zn complexes, we computed the free energies for deprotonating ImH in tetrahedral $[\text{ZnW}_{3-i}\text{L}_i\text{ImH}]$ ($i = 1, 2$) complexes in various media, characterized by a dielectric constant ranging from 1 to 80. The ligand L is MeS^- , ImH, or acetate (Ace^-) to model the most commonly occurring first-shell residues in Zn-binding sites, which, in order of decreasing frequency, are Cys, His, and Asp/Glu.¹⁹ The resulting free energies relative to those of the reference reaction, $[\text{ZnW}_3\text{ImH}]^{2+} \rightarrow [\text{ZnW}_3\text{Im}]^+ + \text{H}^+$, are summarized in Table 4.

(i) First-Shell Ligand Effects. The gas-phase ΔG^1 free energies, which are dominated by the respective ΔH^1 term, monotonically increase as a water molecule in the $[\text{ZnW}_3\text{ImH}]^{2+}$ complex is replaced by ImH, MeCOO^- , and MeS^- , respectively (Table 4, positive $\Delta\Delta G^1$). The observed positive $|\Delta\Delta G^1|$ is mainly because, relative to water, the nonaqua ligands are more polarizable and can therefore donate more charge to Zn than can water. This lowers the positive charge on Zn, which makes the metal less effective in stabilizing the negatively charged Im⁻ in the deprotonated $[\text{ZnW}_2\text{LIm}]^+$ complexes (L = ImH, MeCOO^- , MeS^-) as compared to the deprotonated reference

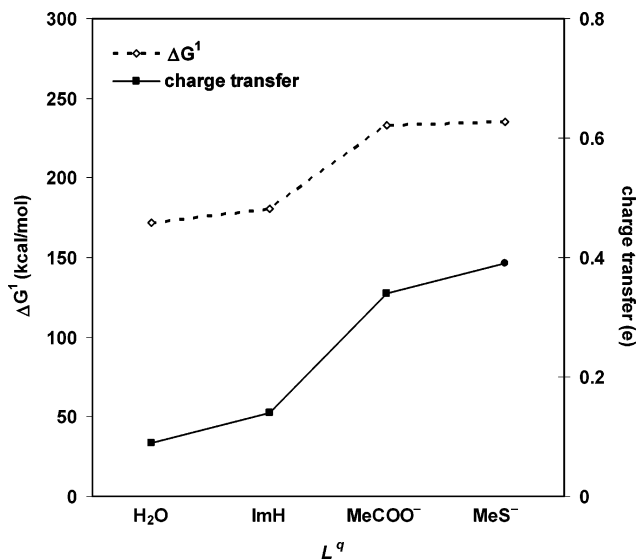


Figure 2. Correlation between the gas-phase deprotonation free energy of $[\text{Zn}(\text{W})_2\text{LImH}]^{2+}$, where $\text{L}^q = \text{H}_2\text{O}^0$, ImH^0 , MeCOO^- , or MeS^- , and the charge transfer from L^q , which is defined by $q(\text{L}) - Q(\text{L})$, where $Q(\text{L})$ is the NBO charge of L in the deprotonated $[\text{Zn}(\text{W})_2\text{LIm}]^{1+}$ complex.

$[\text{ZnW}_3\text{Im}]^+$ complex. The ΔG^1 increase for replacing H_2O with negatively charged $\text{MeCOO}^-/\text{MeS}^-$ (~62–64 kcal/mol) is significantly greater than that for replacing H_2O with neutral ImH (~9 kcal/mol). This is mainly because a negatively charged Zn ligand can donate more charge to the Zn dication than a neutral one, as evidenced by a charge transfer of 0.39e/0.34e from $\text{MeS}^-/\text{MeCOO}^-$ as compared to a charge transfer of 0.14e/0.09e from ImH/ H_2O in the deprotonated metal complex. Interestingly, the observed order in the $|\Delta\Delta G^1|$ correlates with the charge-donating ability of the ligand in the deprotonated metal complex, which increases in the order: $\text{H}_2\text{O} < \text{ImH} < \text{MeCOO}^- < \text{MeS}^-$ (see Figure 2).

(ii) Solvation Effects. As the dielectric constant increases, the unfavorable effect of a polarizable, nonaqua Zn ligand in lowering the metal's positive charge is dramatically attenuated. When $\epsilon \leq 4$, the $\Delta\Delta G$ differences remain positive, but in aqueous solution, they become quite negative for the last two reactions in Table 4. The latter is mainly due to the smaller desolvation penalty of the monocationic $[\text{ZnW}_2\text{LImH}]^+$ (L = MeCOO^- , MeS^-) reactant as compared to the reference dicationic $[\text{ZnW}_3\text{ImH}]^{2+}$ complex, which overcompensates for the poorer solvation of the neutral $[\text{ZnW}_2\text{LIm}]^0$ product relative to the reference monocationic $[\text{ZnW}_3\text{Im}]^+$ complex. These results show that the effect of a Zn ligand on the protonation

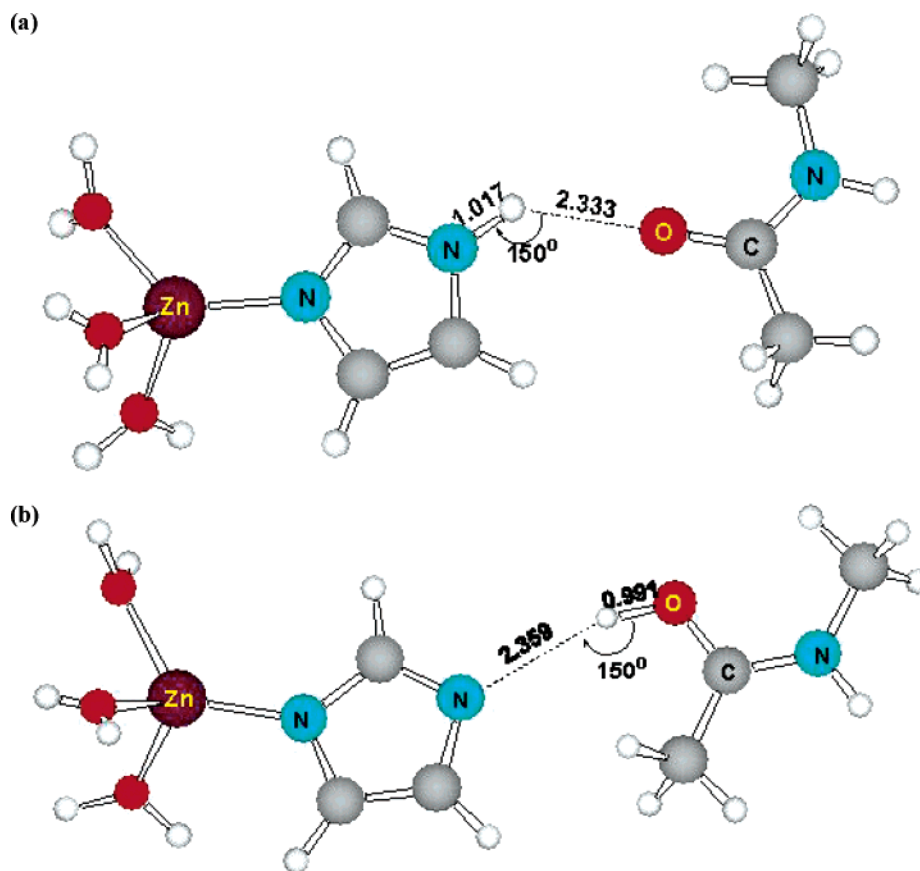


Figure 3. Ball-and-stick diagrams of the restrained optimized structures of the (a) $\{[\text{ZnW}_3\text{ImH}]\cdot\text{MeCONHMe}\}^{2+}$ and (b) $\{[\text{ZnW}_3\text{Im}]\cdot\text{MeCOHNHMe}\}^{2+}$ complexes.

state of the Zn-bound His depends on the solvent accessibility of the metal-binding site. In buried sites, replacing a Zn-bound water molecule with a more polarizable, neutral/negatively charged ligand impedes ionization of the Zn-bound ImH by lowering the positive charge on Zn. On the other hand, in solvent-exposed sites, replacing a Zn-bound water molecule in a dicationic Zn complex with a negatively charged ligand facilitates deprotonation of the Zn-bound ImH by decreasing the net positive charge and thus desolvation penalty of the protonated metal complex.

(3) Effect of the Second-Shell Ligands and the Dielectric Medium. As the two most common second-shell partners of Zn-bound His are the backbone peptide group (via its carbonyl oxygen) and Asp/Glu (via its carboxylate oxygen),¹⁹ we next assessed how these second-shell ligands, modeled respectively by MeCONHMe and MeCOO⁻, affect the Zn-bound His protonation state. The geometries of the protonated $\{[\text{ZnW}_3\text{ImH}]\cdot\text{L}\}^{2+}$ and deprotonated $\{[\text{ZnW}_3\text{Im}]\cdot\text{L}\}^{2+}$ (L = MeCONHMe, MeCOO⁻) complexes were optimized with $R_{\text{N-H}}$, $R_{\text{H-O}}$, and $\theta_{\text{N-H-O}}$ fixed at the values shown in Figures 3 and 4 to restrain the proton to the ImH nitrogen and the second-shell oxygen. Note that the N–H distance of 1.017 Å and the H–O distance of 0.991 Å are typical equilibrium S-VWN/SDD distances obtained for the fully optimized isolated ImH⁰ and MeCOHNHMe⁺ ligands, respectively.

(i) Second-Shell Ligand Effects. In the gas phase, MeCONHMe acts as a hydrogen-bond acceptor of ImH in the absence and presence of Zn, as transferring a ImH proton to the carbonyl oxygen is unfavorable (Table 5, reactions 1 and 2: positive

ΔG^1). In analogy to MeCONHMe, a negatively charged acetate prefers to hydrogen bond with ImH in the absence of Zn in the gas phase: the energy difference between Im^{δ-}–MeCOOH and ImH–MeCOO^{δ-} is 11.3 kcal/mol (Table 5, reaction 3), which is in qualitative agreement with that (16.8 kcal/mol) computed at the B3-LYP/6-311+G(d,p)//B3-LYP/6-311+G(2d,2p) level in previous work.³⁴ However, in the presence of Zn, geometry optimization of the $\{[\text{ZnW}_3\text{ImH}]\cdot\text{Ace}\}^+$ complex (Figure 4a) with $R_{\text{N-H}} = 1.017$ Å, $R_{\text{H-O}} = 2.333$ Å, and $\theta_{\text{N-H-O}} = 150^\circ$ led to spontaneous proton transfer and a $\{[\text{ZnW}_3\text{Im}]\cdot\text{AceH}\}^+$ complex (Figure 4b) with $R_{\text{N-H}} = 2.365$ Å and $R_{\text{H-O}} = 0.985$ Å. The corresponding gas-phase energy for transferring the Zn-bound ImH proton to the second-shell carboxylate oxygen is favorable (–29.6 kcal/mol, Table 5) presumably because charge–charge–dipole electrostatic interactions in Zn^{δ+}⋯Im^{δ-}⋯MeCOOH are much more favorable than charge–dipole–charge interactions in Zn^{δ+}⋯ImH⋯MeCOO^{δ-}.

(ii) Solvation Effects. Solvation effects do not change the trends observed in the gas phase (Table 5, ΔG^x , $x \geq 2$, retain the same sign as ΔG^1). Therefore, in the absence of Zn, both MeCONHMe and MeCOO⁻ prefer to hydrogen bond with ImH. However, in the presence of Zn, a negatively charged second-shell carboxylate group acts as a proton acceptor for the first-shell ImH in the $\{[\text{ZnW}_3\text{ImH}]\cdot\text{Ace}\}^+$ complex, whereas a neutral second-shell backbone group acts as a hydrogen-bond acceptor, irrespective of the solvent accessibility of the Zn complex.

(4) Combined Effect of the First- and Second-Shell Ligands and the Dielectric Medium. As the peptide backbone

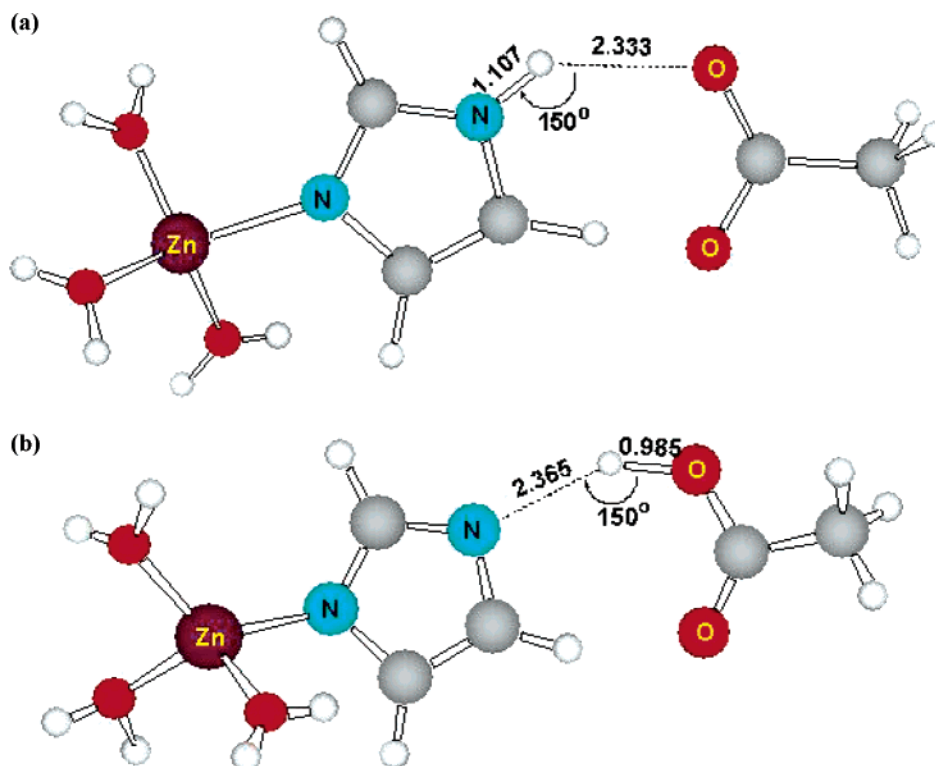


Figure 4. Ball-and-stick diagrams of the restrained optimized structures of the (a) $\{[ZnW_3ImH] \cdot Ace\}^+$ and (b) $\{[ZnW_3Im] \cdot AceH\}^+$ complexes.

Table 5. Effect of the Second-Shell Ligands and the Dielectric Medium on the Proton Transfer ΔG^x (in kcal/mol) of Zn^{2+} -Free and Zn^{2+} -Bound ImH^a

| reactant ^b | product ^b | $\Delta G^{1,c}$ | ΔG^2 | ΔG^4 | ΔG^{80} |
|---|--------------------------------------|------------------|--------------|--------------|-----------------|
| 1. $[ImH \cdots MeCONHMe]^0$ | $[Im \cdots MeCHONHMe]^0$ | 54.3 | 51.1 | 48.9 | 45.9 |
| 2. $\{[ZnW_3ImH] \cdot MeCONHMe\}^{2+}$ | $\{[ZnW_3Im] \cdot MeCHONHMe\}^{2+}$ | 5.7 | 10.6 | 13.2 | 15.6 |
| 3. $[ImH \cdots Ace]^-$ | $[Im \cdots AceH]^-$ | 11.3 | 12.7 | 14.2 | 16.9 |
| 4. $\{[ZnW_3ImH] \cdot Ace\}^+$ | $\{[ZnW_3Im] \cdot AceH\}^+$ | -29.6 | -22.5 | -16.0 | -4.4 |

^a See footnote *a* of Table 4. ^b The R_{N-H} , R_{H-O} , and θ_{N-H-O} values in the reactant and product complexes were fixed, as shown in Figures 3 and 4. ^c $\Delta G^1 \approx \Delta E^1$.

Table 6. Combined Effects of the First- and Second-Shell Ligands and the Dielectric Medium on the Proton Transfer ΔG^x (in kcal/mol) of Zn^{2+} -Bound ImH^a

| reactant | product | ΔG^1 | ΔG^2 | ΔG^4 | ΔG^{80} |
|---------------------------------------|------------------------------------|--------------|--------------|--------------|-----------------|
| 1. $\{[ZnW(ImH)_2ImH] \cdot Ace\}^+$ | $\{[ZnW(ImH)_2Im] \cdot AceH\}^+$ | -30.1 | -21.2 | -15.7 | -8.6 |
| 1. $\{[ZnW_2MeSImH] \cdot Ace\}^0$ | $\{[ZnW_2MeSIm] \cdot AceH\}^0$ | -17.9 | -10.4 | -5.4 | 1.4 |
| 3. $\{[ZnW AceImHImH] \cdot Ace\}^0$ | $\{[ZnW AceImHIm] \cdot AceH\}^0$ | -15.4 | -8.9 | -4.6 | 1.1 |
| 4. $\{[ZnW MeSImHImH] \cdot Ace\}^0$ | $\{[ZnW MeSImHIm] \cdot AceH\}^0$ | -7.3 | 0.2 | 5.0 | 11.3 |
| 5. $\{[ZnW(MeS)_2ImH] \cdot Ace\}^-$ | $\{[ZnW(MeS)_2Im] \cdot AceH\}^-$ | -0.2 | 2.1 | 4.2 | 8.6 |
| 6. $\{[ZnOH(ImH)_2ImH] \cdot Ace\}^0$ | $\{[ZnOH(ImH)_2Im] \cdot AceH\}^0$ | -5.6 | 1.2 | 5.4 | 9.4 |
| 7. $\{[ZnOHAceImHImH] \cdot Ace\}^-$ | $\{[ZnOHAceImHIm] \cdot AceH\}^-$ | 3.6 | 6.3 | 8.4 | 11.8 |

^a See footnotes to Table 5.

carbonyl oxygen can only act as a hydrogen-bond acceptor, whereas an Asp/Glu carboxylate oxygen, which is often found within 3.5 Å of the Zn-bound ImH nitrogen in the common catalytic sites,¹⁹ could also act as a proton acceptor, we next elucidated how both the first-shell Zn ligands and the second-shell carboxylate group affect the protonation state of Zn-bound His. To this end, we computed the free energies for transferring the first-shell imidazole proton to the second-shell carboxylate oxygen in various Zn complexes, modeling the three general types of catalytic Zn cores, viz., $[Zn(H_2O)(His)_3]$, $[Zn(H_2O)(Asp/Glu)(His)_2]$, and $[Zn(H_2O)(Cys)_2(His)]$ (Table 6, reactions 1, 3, and 5). As the Zn-bound water in the $[Zn(H_2O)(His)_3]$ or $[Zn(H_2O)(Asp/Glu)(His)_2]$ core is known to be deprotonated at

high pH (>7) in enzymes such as carbonic anhydrase^{31,75–77} and carboxypeptidase A,⁷⁸ a deprotonated Zn-bound water (OH^-) was also modeled in these two types of Zn catalytic cores (Table 6, reactions 6 and 7). The geometries of the Zn complexes were optimized with R_{N-H} , R_{H-O} , and θ_{N-H-O} fixed at the values shown in Figures 3 and 4 (see above).

(i) First- and Second-Shell Ligand Effects. The trends in the gas-phase proton-transfer free energies in Table 6 correlate with the charge-donating ability of the Zn ligand, which

(75) Silverman, D.; Vincent, S. H. *CRC Crit. Rev. Biochem.* **1983**, *14*, 207.

(76) Silverman, D. N.; Lindsog, S. *Acc. Chem. Res.* **1988**, *21*, 30.

(77) Lindsog, S. *Carbonic Anhydrase In Zinc Enzymes*; Wiley: New York, 1983.

(78) Lipscomb, W. N.; Strater, N. *Chem. Rev.* **1996**, *96*, 2375.

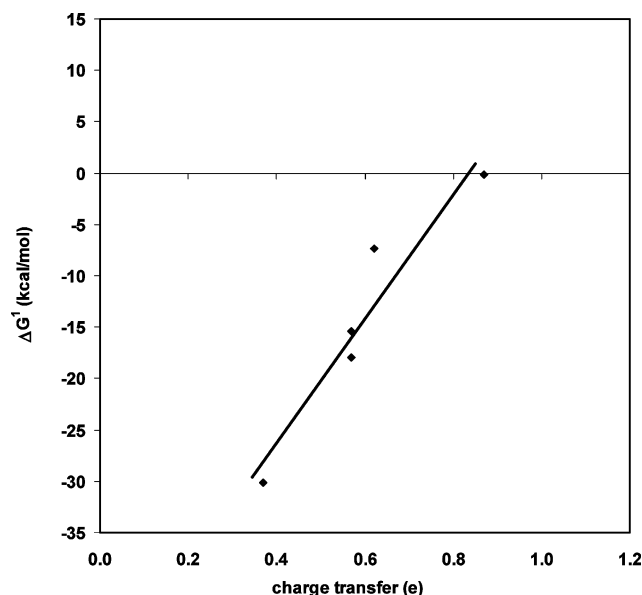


Figure 5. Correlation between the proton-transfer energies (ΔG^1) for the reactions in Table 6 and the net charge transferred by the L_1 , L_2 , and L_3 ligands in the deprotonated $\{[ZnL_1L_2L_3Im]\cdot AceH\}$ complex. The charge transferred by each L_i ligand is obtained from Figure 2, where it is 0.09e for H_2O , 0.14e for ImH, 0.34e for $MeCOO^-$, and 0.39e for MeS^- .

increases as $H_2O < ImH < MeCOO^- < MeS^-$ (see above and Figure 2). This is shown in Figure 5, which plots ΔG^1 against the sum of the charges transferred by the L_1 , L_2 , and L_3 ligands in the deprotonated $\{[ZnL_1L_2L_3Im]\cdot AceH\}$ complex. When the charge transferred by each L_i ligand is obtained from Figure 2 (0.09e for H_2O , 0.14e for ImH, 0.34e for $MeCOO^-$, and 0.39e for MeS^-), the ΔG^1 value in Table 6 is correlated with the net charge transferred by the L_1 , L_2 , and L_3 ligands with a linear correlation coefficient, $r^2 = 0.91$. When the Zn-bound water in the modeled $\{[ZnW AceImHImH]\cdot Ace\}^0$ catalytic Zn complex is deprotonated, ΔG^1 becomes unfavorable (Table 6, last reaction). The trend in ΔG^1 thus reflects the extent to which Zn can stabilize the deprotonated Im^- : charge transfer from the first-shell ligands reduces the positive charge on Zn, which in turn reduces favorable charge–charge $Zn^{\delta+}\cdots Im^{\delta-}$ interactions in the deprotonated complex.

(ii) Solvation Effects. As the dielectric constant increases, the ΔG^x ($x = 2, \dots, 80$) values become more unfavorable (Table 6) mainly because the metal complex with an outer-shell COO^- is better solvated than the deprotonated metal complex with an outer-shell $COOH$. Consequently, the second-shell carboxylate group can act either as a proton/hydrogen-bond acceptor depending on the type and solvent accessibility of the catalytic Zn site. In catalytic $[Zn(H_2O)(His)_3]$ cores, where charge transfer from the neutral imidazoles has not significantly reduced the Lewis acid ability of Zn, a second-shell carboxylate could act as a proton acceptor for the first-shell ImH regardless of the solvent exposure of the Zn-binding site (Table 6, reaction 1: negative ΔG^x , $x \leq 80$). Replacing one of the His in the $[Zn(H_2O)(His)_3]$ cores by an Asp/Glu reduces the ability of Zn to act as a Lewis acid, but the second-shell COO^- may still act as a proton acceptor in buried $[Zn(H_2O)(Asp/Glu)(His)_2]$ catalytic sites (Table 6, reaction 3: negative ΔG^x , $x \leq 4$). In catalytic $[Zn(H_2O)(Cys)_2(His)]$ cores, where charge transfer from the two negatively charged Cys has significantly reduced the positive charge on Zn, the Zn-bound ImH prefers to hydrogen bond with

the second-shell COO^- in buried or solvent-exposed sites (Table 6, reaction 5: positive ΔG^x , $x > 2$). For all three common types of catalytic Zn cores, the second-shell Asp/Glu side chain prefers to hydrogen bond to the first-shell ImH if the Zn-bound H_2O is deprotonated (Table 6, reactions 6 and 7: positive ΔG^x , $x > 2$).

Effect of the Second-Shell Asp/Glu on the Zn-Bound Water Protonation State. To see if the Asp/Glu in the Zn–His–Asp/Glu triad could modulate the pK_a of the Zn-bound water (see Introduction), we computed the free energy for deprotonating the Zn-bound water in the $[ZnW(ImH)_3]^{2+}$, $[ZnW Ace(ImH)_2]^+$, and $[ZnW(MeS)_2ImH]^0$ complexes, modeling the three general types of catalytic Zn cores, in the absence and presence of a second-shell carboxylate group (Table 7). All of the geometries of the Zn complexes in Table 7 were fully optimized. Hence, the histidine interacting with the second-shell carboxylate in the $\{[ZnW(ImH)_3]\cdot Ace\}^+$, $[ZnW Ace(ImH)_2]\cdot Ace\}^0$, or $\{[ZnOH(ImH)_3]\cdot Ace\}^0$ complex is deprotonated to $\{[ZnW(ImH)_2Im]\cdot AceH\}^+$, $[ZnW AceImHIm]\cdot AceH\}^0$, or $\{[ZnOH(ImH)_2Im]\cdot AceH\}^0$, respectively (Table 7, reactions 2 and 4), as proton transfer is thermodynamically favorable (Table 6, reactions 1, 3, and 6: negative ΔG^1).

The results in Table 7 show that the Asp/Glu in the Zn–His–Asp/Glu triad exerts opposite effects on the protonation state of the Zn-bound water depending on whether the metal-binding site is buried or solvent exposed. In the gas phase, the interaction between an outer-shell carboxylate group and a Zn-bound His significantly increases the deprotonation free energy of the Zn-bound water (Table 7, reactions 2, 4, and 6: positive $\Delta\Delta G^1$). This is probably because the negatively charged carboxylate group destabilizes the deprotonated metal complex via repulsive Coulombic interactions with the Zn-bound hydroxide. As the dielectric constant increases, the unfavorable effect of the outer-shell carboxylate group on the Zn-bound water deprotonation is dramatically diminished and is reversed in aqueous solution where $\Delta\Delta G^{80}$ values become negative. The latter is due to (1) the smaller desolvation penalty of the reactant complex with net charge Q (≥ 0) as compared to the respective reference complex with net charge $Q + 1$ (Table 7, reactions 2 and 4) and/or (2) the better solvation of the product with net charge $-(Q+1)$ as compared to that of the reference product with net charge $-Q'$ (Table 7, reactions 4 and 6). For a certain dielectric constant x , the $\Delta\Delta G^x$ difference between the Zn complexes with and without a second-shell carboxylate group in Table 7 is close to zero, suggesting that the effect of the Zn–His–Asp/Glu interaction on the Zn-bound water pK_a in certain Zn sites is negligible.

Discussion

Factors Governing the Zn-Bound Histidine Protonation State in Proteins: Role of Asp/Glu in the Zn–His–Asp/Glu Triad as a Hydrogen-Bond or Proton Acceptor. To the best of our knowledge, this is the first systematic study of the various factors affecting the protonation state of the Zn-bound His in proteins, which is found here to be governed mainly by (1) the nature of the second-shell residue, (2) the nature of the other Zn ligands, and (3) the solvent accessibility of the Zn-binding site. Not any second-shell ligand with a hydrogen acceptor atom can alter the protonation state of the Zn-bound ImH. The backbone carbonyl oxygen may not change the Zn–

Table 7. Effect of a Second-Shell Carboxylate on the Deprotonation ΔH^1 and ΔG^x Values (kcal/mol) of Zn-Bound Water for Media of Various Dielectric Constants x^a

| reactant | product + H ⁺ | $\Delta\Delta H^1$ | $\Delta\Delta G^1$ | $\Delta\Delta G^2$ | $\Delta\Delta G^4$ | $\Delta\Delta G^{80}$ |
|---|---|--------------------|--------------------|--------------------|--------------------|-----------------------|
| 1. [ZnW(ImH) ₃] ²⁺ | [ZnOH(ImH) ₃] ⁺ | 0.0 | 0.0 | 0.0 | 0.0 | 0.0 |
| 2. {[ZnW(ImH) ₂ Im]·AceH} ⁺ | {[ZnOH(ImH) ₂ Im]·AceH} ⁰ | 54.7 ^b | 53.3 ^b | 20.1 ^b | 3.7 ^b | -11.1 ^b |
| 3. [ZnWAce(ImH) ₂] ⁺ | [ZnOHAce(ImH) ₂] ⁰ | 0.0 | 0.0 | 0.0 | 0.0 | 0.0 |
| 4. {[ZnWAceImHIm]·AceH} ⁰ | {[ZnOHAce(ImH) ₂ Im]·Ace} ⁻ | 51.2 ^c | 50.5 ^c | 16.4 ^c | -2.3 ^c | -20.2 ^c |
| 5. [ZnW(MeS) ₂ ImH] ⁰ | [ZnOH(MeS) ₂ ImH] ⁻ | 0.0 | 0.0 | 0.0 | 0.0 | 0.0 |
| 6. {[ZnW(MeS) ₂ ImH]·Ace} ⁻ | {[ZnOH(MeS) ₂ ImH]·Ace} ²⁻ | 48.0 ^d | 47.5 ^d | 15.2 ^d | -1.2 ^d | -16.5 ^d |

^a See footnote *a* of Table 4. ^b The computed thermodynamic parameters are relative to those of reaction 1, whose ΔH^1 , ΔG^1 , ΔG^2 , ΔG^4 , and ΔG^{80} values are equal to 176.7, 170.8, 103.1, 62.5, and 3.5 kcal/mol, respectively. ^c The computed thermodynamic parameters are relative to those of reaction 3, whose ΔH^1 , ΔG^1 , ΔG^2 , ΔG^4 , and ΔG^{80} values are equal to 261.5, 253.9, 149.0, 89.9, and 11.5 kcal/mol, respectively. ^d The computed thermodynamic parameters are relative to those of reaction 5, whose ΔH^1 , ΔG^1 , ΔG^2 , ΔG^4 , and ΔG^{80} values are equal to 332.7, 325.1, 181.3, 101.4, and 3.2 kcal/mol, respectively.

bound ImH protonation state, as it prefers to hydrogen bond with the Zn-bound ImH. On the other hand, the Asp/Glu carboxylate oxygen can act either as a hydrogen-bond or proton acceptor of the Zn-bound ImH, depending on the electronic properties of the other Zn ligands and the solvent accessibility of the Zn site. Poor charge donors such as water molecules do not significantly reduce the metal charge, allowing Zn to act as a Lewis acid in stabilizing the negatively charged Im⁻ (Table 5, last reaction). In contrast, good charge donors such as CH₃S⁻ can competitively transfer charge to Zn, thus decreasing the ability of Zn to stabilize Im⁻ (Table 6, reactions 4 and 5). Furthermore, solvation effects generally disfavor transfer of the Zn-bound ImH proton to the second-shell carboxylate oxygen because the Zn complex with a negatively charged COO⁻ group in the outer shell is better solvated than that with a neutral COOH group (Table 6). Hence, the Asp/Glu side chain has a greater propensity to hydrogen bond with the Zn-bound ImH in solvent-accessible sites, whereas it has a greater propensity to accept a proton from the Zn-bound ImH in buried sites.

Protonation State of the Zn-Bound His in Proteins. The Zn-bound ImH may be deprotonated if its free nitrogen is within hydrogen-bonding distance (≤ 3.5 Å) of a second-shell carboxylate oxygen, and the Zn is either (a) hydrated (Table 5, last reaction: negative ΔG^x , $x \geq 2$) or (b) retains at least one water molecule and is coordinated to only neutral amino acids (Table 6, reaction 1: negative ΔG^x , $x \leq 80$). On the other hand, the Zn-bound ImH is likely to be neutral if (1) its free nitrogen is not within hydrogen-bonding distance of a second-shell ligand with a hydrogen acceptor atom (Table 4, absolute $\Delta G^x \gg 5$ kcal/mol for $x < 80$); (2) its free nitrogen is within hydrogen-bonding distance of a second-shell carbonyl oxygen (Table 5, reaction 2: positive ΔG^x , $x \geq 2$); and (3) its free nitrogen is within hydrogen-bonding distance of a second-shell carboxylate oxygen, but Zn is bound to only one water and one or two Cys⁻ (Table 6, reactions 4 and 5: positive ΔG^x , $x \geq 4$) or no neutral water molecules (Table 6, reactions 6 and 7: positive ΔG^x , $x > 2$). The latter suggest that at high pH (> 8), where the Zn-bound H₂O would be deprotonated in the catalytic [Zn(OH)(His)₃] core of carbonic anhydrase II and the [Zn(OH)(Asp/Glu)(His)₂] core of carboxypeptidase A, proton transfer from the Zn-bound His to the outer-shell Asp/Glu is unlikely.

Role of Asp/Glu in the Zn–His–Asp/Glu Triad in Modulating the Basicity/Nucleophilicity of Zn-Bound Water. In the absence of outer-shell Asp/Glu residues interacting with the first-shell His and water, the Zn-bound water in the common catalytic Zn sites is unlikely to be deprotonated at physiological pH especially if the metal-binding site is buried (Table 7, reactions 1, 3, and 5: positive ΔG^x). In fact, the Zn-bound water

Table 8. NBO Charges on the Zn Ligands and the Outer-Shell MeCOO⁻ in Model Zn Sites^a

| dyad | | | | triad | | | |
|--------------------|--------------|--------------------|--------------|--------------------|--------------|--------------------|--------------|
| ligand | <i>Q</i> (e) | ligand | <i>Q</i> (e) | ligand | <i>Q</i> (e) | ligand | <i>Q</i> (e) |
| Zn | 1.57 | Zn | 1.55 | Zn | 1.56 | Zn | 1.55 |
| W | +0.08 | OH ⁻ | -0.77 | W | +0.02 | OH ⁻ | -0.77 |
| ImH | +0.12 | ImH | +0.09 | ImH | +0.11 | ImH | +0.04 |
| ImH | +0.12 | ImH | +0.07 | ImH | +0.12 | ImH | +0.05 |
| ImH | +0.12 | ImH | +0.06 | Im ⁻ | -0.67 | Im ⁻ | -0.64 |
| first-shell | +0.44 | first-shell | -0.55 | first-shell | -0.42 | first-shell | -0.59 |
| | | | | MeCOOH | -0.14 | MeCOO ⁻ | -0.23 |
| Zn | 1.56 | Zn | 1.53 | Zn | 1.55 | Zn | 1.55 |
| W | -0.12 | OH ⁻ | -0.77 | W | -0.11 | OH ⁻ | -0.80 |
| MeCOO ⁻ | -0.64 | MeCOO ⁻ | -0.80 | MeCOO ⁻ | -0.66 | MeCOO ⁻ | -0.85 |
| ImH | +0.10 | ImH | +0.02 | ImH | +0.07 | ImH | +0.02 |
| ImH | +0.10 | ImH | +0.02 | Im ⁻ | -0.63 | ImH | -0.12 |
| first-shell | -0.56 | first-shell | -1.53 | first-shell | -1.33 | first-shell | -1.75 |
| | | | | MeCOOH | -0.22 | MeCOO ⁻ | -0.79 |
| Zn | 1.27 | Zn | 1.31 | Zn | 1.29 | Zn | 1.32 |
| W | -0.06 | OH ⁻ | -0.79 | W | -0.06 | OH ⁻ | -0.80 |
| MeS ⁻ | -0.67 | MeS ⁻ | -0.74 | MeS ⁻ | -0.67 | MeS ⁻ | -0.80 |
| MeS ⁻ | -0.60 | MeS ⁻ | -0.75 | MeS ⁻ | -0.68 | MeS ⁻ | -0.78 |
| ImH | +0.05 | ImH | -0.03 | ImH | -0.12 | ImH | -0.11 |
| first-shell | -1.28 | first-shell | -2.31 | first-shell | -1.53 | first-shell | -2.49 |
| | | | | MeCOO ⁻ | -0.76 | MeCOO ⁻ | -0.84 |

^a All geometries were fully optimized at the S-VWN/SDD level.

ΔG^4 in model [Zn(H₂O)(Asp/Glu)(His)₂] and [Zn(H₂O)(Cys)₂(His)] cores (90 and 101 kcal/mol, respectively) are greater than those in model [Zn(H₂O)(His)₃] cores (63 kcal/mol). This is consistent with the experimental finding that substitution of the Zn-bound His with Asp/Cys increased the Zn-bound water *pK_a* substantially.³² The presence of an outer-shell Asp/Glu interacting with the Zn-bound His could facilitate deprotonation of the Zn-bound water at pH > 7 only if the Zn-binding site is solvent exposed (Table 7, negative $\Delta\Delta G^{80}$ for reactions 2, 4, and 6). In partially buried or deeply buried sites, the Zn–His–Asp/Glu interaction may not help to deprotonate the Zn-bound water (Table 7, small or positive $\Delta\Delta G^x$ for reactions 2, 4, and 6). This suggests that other interactions, such as those between the Zn-bound water and a second-shell Asp/Glu, are needed to promote ionization of a Zn-bound water to hydroxide in buried/partially buried sites.²³

Role of Asp/Glu in the Zn–His–Asp/Glu Triad in Forming an Anionic Hole and Promoting Zn Binding. The second-shell Asp/Glu residue may also play an important role in creating an anionic hole by increasing the negative charge of the His in the Zn–His–Asp/Glu triad. This is evidenced by the NBO charges on the Zn ligands of the fully optimized Zn complexes in Table 8, where the His in the Zn–His–Asp/Glu triad is protonated/deprotonated according to the computed ΔG^1 values in Table 6. Thus, the His in the Zn–His–Asp/Glu triad is

deprotonated in the $\{[\text{ZnW}(\text{ImH})_3]\cdot\text{Ace}\}^+$, $\{[\text{ZnOH}(\text{ImH})_3]\cdot\text{Ace}\}^0$, and $\{[\text{ZnW}(\text{Ace})(\text{ImH})_2]\cdot\text{Ace}\}^0$ complexes (negative ΔG^\ddagger , Table 6), but is protonated in the $\{[\text{ZnOH}(\text{Ace})(\text{ImH})_2]\cdot\text{Ace}\}^-$, $\{[\text{ZnW}(\text{MeS})_2(\text{ImH})]\text{Ace}\}^-$, and $\{[\text{ZnOH}(\text{MeS})_2(\text{ImH})]\text{Ace}\}^{2-}$ complexes in Table 8. When ImH is near a second-shell MeCOO^- , its charge in $[\text{ZnW}(\text{ImH})_3]$ (-0.67e), $[\text{ZnW}(\text{Ace})(\text{ImH})_2]$ (-0.63e), or $[\text{ZnW}(\text{MeS})_2(\text{ImH})]$ (-0.12e) sites is much more negative than the respective charge in the absence of a second-shell MeCOO^- (Table 8, compare columns 6 and 2). Likewise, the triad ImH charge in $[\text{ZnOH}(\text{ImH})_3]$ (-0.64e), $[\text{ZnOH}(\text{Ace})(\text{ImH})_2]$ (-0.12e), or $[\text{ZnOH}(\text{MeS})_2(\text{ImH})]$ (-0.11e) sites is more negative than the respective dyad ImH charge (Table 8, compare columns 8 and 4). Furthermore, the presence of a second-shell MeCOO^- increases the net negative charge of the first-shell ligands (Table 8, compare dyad and triad first-shell charges), which results in favorable charge–charge interactions with the Zn cation.

The finding that the Asp/Glu side chain in the Zn–His–Asp/Glu triad can increase the negative charge of its partner, His, and create an anionic hole that may stabilize a cation in buried cavities is consistent with previous theoretical and experimental results. The active site of liver horse alcohol dehydrogenase has been modeled by $[\text{Zn}(\text{EtO})(\text{MeS})_2(\text{ImH})]^-$ with the ethanolate (EtO) hydrogen bonded to ethanol, which in turn is hydrogen bonded to nicotinamide nucleoside (modeling the NAD^+ cofactor). Electron density distributions of this model complex with and without an acetate hydrogen bonded to the Zn-bound ImH show that addition of the carboxylate group causes a transfer of negative charge to the Zn-bound ImH, which in turn donates electron density to the Zn, and to a lesser extent to the Zn-bound ethanolate.³⁵ In the $[\text{Zn}(\text{H}_2\text{O})(\text{His})_3]$ core of human carbonic anhydrase, the outer-shell partners of the Zn-bound His⁹⁴, His⁹⁶, and His¹¹⁹ are the Gln⁹² side chain, the Asn²⁴⁴ backbone, and the Glu¹¹⁷ side chain, respectively. The Zn-dissociation constant for the His¹¹⁹ → Ala mutant ($K_D = 1000$ nM) is significantly higher than that for the His⁹⁴ → Ala ($K_D = 270 \pm 50$ nM) and His⁹⁶ → Ala ($K_D = 100$ nM) mutants, while the Zn-binding affinity of the Glu¹¹⁷ → Ala mutant is 10-fold less than that of the wild-type protein (see Introduction).³² The latter result had been interpreted to imply that the Glu¹¹⁷⋯His¹¹⁹ interaction orients the His in an optimal position for coordinating to Zn, hence reducing the entropic penalty for

Zn binding.^{1,12,27,33,79} However, the theoretical results in this and previous work^{31,35} suggest that the observed loss in Zn-binding affinity of the Glu¹¹⁷ → Ala mutant could also be due to reduced favorable electrostatic interactions between the metal and its first-shell ligands in the mutant relative to those in the wild-type protein.

Biological Significance. The results herein provide valuable knowledge in rational design of Zn-binding sites and modeling of metalloproteins. For example, Zn-binding affinity could be enhanced by mutating residues in the vicinity of a Zn-bound His with few/no hydrogen-bonding interactions to an Asp/Glu provided that the net charge of the metal and its first-shell ligands is positive or neutral. In fact, this expectation has been borne out in the designed cationic $[\text{Zn}(\text{His})_3\text{Cys}]$ site of a B1 domain variant of IgG-binding protein G, where mutating Val/Leu residues near the coordinating imidazoles to Asp/Glu enhanced Zn-binding affinity (see Introduction).³⁰ As another example, the Zn-bound water of a cationic or neutral Zn complex could be deprotonated by (i) mutating its non-hydrogen-bonded neighbors to an Asp/Glu if the metal-binding site is partially/fully buried, or (ii) mutating non-hydrogen-bonded residues in the vicinity of the Zn-bound histidine to an Asp/Glu if the metal-binding site is partially/fully solvent exposed (see above and Table 7). Such mutations may enhance catalytic activity if nucleophilic attack of a Zn-bound hydroxide were rate-limiting. Because of the important roles of the second-shell Asp/Glu, it is critical to include not only the metal's first-shell interactions, but also the interactions between the metal's first and second shells in quantum mechanical/molecular mechanical modeling of metalloproteins and in engineering nativelike metal-binding sites.

Acknowledgment. We thank Todor Dudev, Hsiu-fong Lu, and Yu-ming Lee for helpful discussions and both referees for helpful, constructive comments. We are grateful to D. Bashford, M. Sommer, and M. Karplus for the program to solve the Poisson equation. This work was supported by the National Science Council, Taiwan (NSC Contract # 92-2113-M-001-032), and the Institute of Biomedical Science, Academia Sinica, Taiwan.

JA038827R

(79) Carver, J. A.; Bradbury, J. H. *Biochemistry* **1984**, *23*, 4890.